

THE QUADRUPLE WOLF-RAYET SYSTEM GP CEPHEI: SPECTRAL TYPES, MASSES, MASS-LOSS RATE, AND COLLIDING WINDS

H. DEMERS, A. F. J. MOFFAT, AND S. V. MARCHENKO¹

Département de Physique, Université de Montréal, C. P. 6128, Succ. Centre-Ville, Montréal, QC H3C 3J7, Canada; and Observatoire du Mont Mégantic; hdemers@astro.umontreal.ca, moffat@astro.umontreal.ca, sergey@astro.wku.edu

K. G. GAYLEY

Department of Physics and Astronomy, University of Iowa, Iowa City, IA 52242; kgg@astro.physics.uiowa.edu

AND

T. MOREL

Inter University Centre for Astronomy and Astrophysics, Post Bag 4, Ganeshkhind, Pune 411007, India; morel@iucaa.ernet.in

Received 2001 December 14; accepted 2002 May 24

ABSTRACT

We have reevaluated the orbital elements for each pair of the quadruple (W-R+O) + (O+O) stellar system GP Cep and propose new spectral types WN60/WCE + O3–6, B0: I + B1: V–III. It is shown that there is only one Wolf-Rayet (W-R) star in GP Cep, contrary to a previous claim. A rate of change $\dot{P} = 1.3 \pm 0.2 \text{ s yr}^{-1}$ is determined for the W-R+O pair, which leads to a new period of 6.6887 days and to a W-R mass-loss rate of $(0.8\text{--}3.0) \times 10^{-5} M_{\odot} \text{ yr}^{-1}$. Masses for this pair are estimated to be $M_{\text{W-R}} \gtrsim 6 M_{\odot}$ and $M_{\text{O}} \gtrsim 21 M_{\odot}$. The effects of wind-wind collision in the W-R+O pair are studied. It is shown that even after allowing for dilution by the OB components of the quadruple system, these effects are not as strong as in the binary V444 Cygni (WN5+O6, $P = 4.212$ days). In GP Cep, the phase-dependent, relatively weak excess emission does not originate in the arms of the bow shock cone. Rather, it emerges from the extra heated portion of the W-R wind facing the hot O companion. The trailing bow shock arm is clearly seen, however, as an enhanced He I absorption component near quadrature at phase ~ 0.73 . An anomalous blueshifted He I absorption is present at phase ~ 0.9 , as is also seen in V444 Cyg, in the WC8+O9 I/O8 III binary γ Velorum and in the LBV-cotype binary R81 (B2.5 Iab:e). A 3.5 day orbit for the eclipsing B star pair is confirmed.

Subject headings: binaries: eclipsing — stars: fundamental parameters — stars: individual (WR 153) — stars: mass loss — stars: Wolf-Rayet

1. INTRODUCTION

GP Cep (WR 153, HD 211853) is a quadruple system (Massey 1981) composed of two stellar binaries: a W-R+O system (pair A, $P = 6.6884$ days) and an O+O system (pair B, $P = 3.4696$ days; Anuk 1994). Both pairs reveal eclipse-like light curves, with only one minimum per cycle in the light curve for pair A and two minima per cycle for pair B (Panov, Altmann, & Seggewiss 2000). Smith, Shara, & Moffat (1996) classified GP Cep as WN60/CE+O6 I. Although Massey (1981) finds only one Wolf-Rayet (W-R) star in the quadruple system, Panov & Seggewiss (1990) claim two W-R components, one in each binary.

In the present study, we mainly target the effects of wind-wind collision (WWC) seen in He I $\lambda 4471$ and in He II $\lambda 4686$. These are the lines in the blue-green region of the optical spectra where the effect is clearest. A procedure developed by Marchenko, Moffat, & Eenens (1998a) was used, in which the W-R component spectrum was separated from the OB spectrum. Having done this, it was possible to isolate the effects of WWC in pair A. This also gave us the opportunity to reevaluate the W-R orbital parameters and to put constraints on the OB stars' spectral types. Along with the abundant spectral data, we also study the photometric observations obtained in many epochs over ~ 40 yr.

For pair A, this leads to a new estimate of the period and its rate of change.

2. OBSERVATIONS AND REDUCTION

All spectra were taken in the summer of 1999 with the 1.6 m telescope and 2048×2048 pixel Loral CCD of the Mont Mégantic Observatory (Québec). The wavelength coverage spans $4250\text{--}5600 \text{ \AA}$ with $\Delta\lambda = 1.86 \text{ \AA}$ 3 pixel resolution (i.e., the FWHM of the instrumental profile). The combination of three consecutive exposures of ~ 10 minutes each gives a typical net signal-to-noise ratio of $S/N \approx 180 \text{ pixel}^{-1}$ in the extracted spectrum in the continuum around 5100 \AA . The reduction was performed using standard IRAF² facilities. This provides us with a total of 99 spectra covering almost all phases spread over an interval of 125 days, with 19 6.7 day cycles covered with various degrees of completeness.

The mean spectrum in the W-R frame is presented in Figure 1a. The journal of observations is given in Table 1, in which column (1) is the heliocentric Julian date; columns (2)–(3) are the phases of each pair in accordance with $T_{0,A} = 2443690.32$ and $P_A = 6.6884$ days (Massey 1981) for pair A and $T_{0,B} = 2443689.16$ and $P_B = 3.4696$ days (Anuk 1994) for pair B; column (4) is the radial velocity

¹ Now at the Department of Physics and Astronomy, Western Kentucky University, Thompson Complex Central Wing, Bowling Green, KY 42101-3576.

² IRAF is distributed by the National Optical Astronomy Observatory, operated by the Association of Universities for Research in Astronomy, Inc., under cooperative agreement with the National Science Foundation.

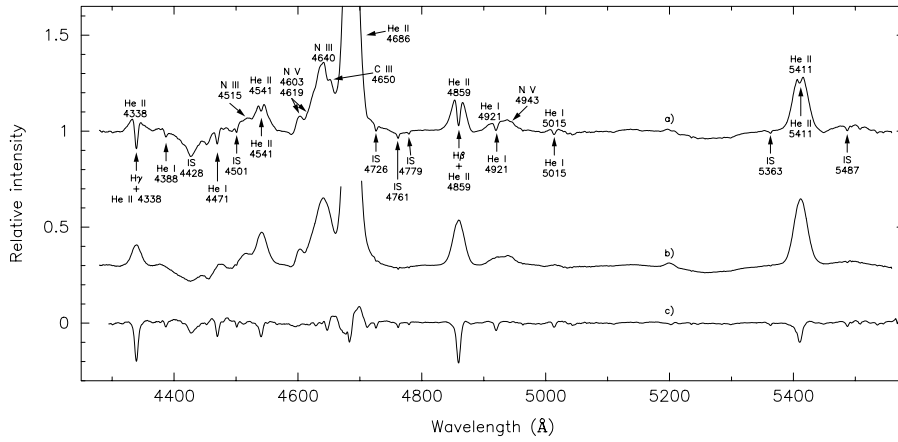


FIG. 1.—Mean spectrum of (a) the four-component spectrum in the frame of the W-R star and (b) the W-R component after removing (c) the spectrum of the O stars. Artifacts seen at $\lambda 4686$ in (c) are the result of the phase-dependent variability of the W-R spectrum caused by the atmospheric eclipses at $\phi \sim 0$ (see text).

(RV) of the W-R component calculated by cross-correlation (see § 3.2); column (5) is the RVs of the three blended OB spectra found by cross-correlation (see § 3.2); and columns (6)–(8) are the RVs of three individual spectral lines from the three blended OB spectra (see § 3.2). Note that $T_{0,A}$ is the time of conjunction when the W-R star is in front.

Added to the complexity of GP Cep being quadruple, the W-R+O subsystem also reveals wind eclipses. In order to account for this fact, all spectra were corrected for continuum-level variations by fitting a light curve to previously published and unpublished photometric data. Nine different photometric data sets spread over ~ 40 yr were used. These were taken from all available publications from 1963 to 2000 and supplemented by our own data set acquired in 1996 at the Observatorio Astronómico Nacional de San Pedro Martír (Mexico). A v filter centered at 5140 \AA with a FWHM of 90 \AA was used. For more details, see Morel et al. (1999). The other data sets come from Hjellming & Hiltner (1963), Stepien (1970), Cherepashchuk (1975), Moffat & Shara (1986), *Hipparcos* (Perryman 1997; Marchenko et al. 1998b), Anuk (1994), Lamontagne et al. (1996), and Panov et al. (2000).

3. RESULTS AND DISCUSSION

We start with the photometric data, since their large quantity offers the best determination of periods and their possible changes with time. Also, proper treatment of the spectra requires knowledge of the continuum level based on the light curves, $m(\phi)$.

3.1. Photometry and Light-Curve Fitting

Since we do not know the precise forms of the light curves of pair A and pair B a priori, we must isolate each pair's light curve separately. We therefore adopted an iterative process to separate them. All data were first phased with pair A's ephemeris from Massey (1981). This revealed a predominantly V-shaped dip centered at $\phi = 0.0$ in all data sets. It therefore appeared reasonable, as a first step, to fit an atmospheric eclipse curve found for a sample of close W-R+O systems (Lamontagne et al. 1996). Then the residuals to this fit were computed and rephased using the ephemeris of pair B from Anuk (1994). This revealed a

double wave per cycle, probably the result of eclipses and/or ellipsoidal variations in this very close system. After fitting a curve to the rephased residuals (see eq. [6] below), this last fit was subtracted from the original data and the process repeated. The two different models used to fit the light curves for each of system A and system B are as follow.

The light curve of pair A was fitted using the model from Lamontagne et al. (1996) of atmospheric eclipse by a spherically symmetric Thomson scattering W-R wind. Under the assumption of a constant W-R wind velocity ($v = v_\infty$), which is generally an adequate approximation in the case of atmospheric eclipses (see Lamontagne et al. 1996), the light curve can be represented by

$$m = m_0 + A \left(\frac{\pi/2 + \arcsin \epsilon}{\sqrt{1 - \epsilon^2}} \right), \quad (1)$$

where

$$A = 1.086k \left(\frac{I_{W-R} + I_{B_1} + I_{B_2}}{I_A} + 1 \right)^{-1}, \quad (2)$$

$$\epsilon = (\sin i) \cos 2\pi(\phi_A - \phi_{0,A}),$$

in which

$$k = \frac{\alpha \sigma_{\text{Th}} \dot{M}}{4\pi m_p v_\infty a}. \quad (3)$$

Here I_{W-R} is the W-R intensity, I_A is the unattenuated intensity of the O star from pair A, I_{B_1} and I_{B_2} are the unattenuated intensities from the stars in pair B, α is the number of free electrons per baryon mass m_p , σ_{Th} is the Thomson single-electron scattering cross section, a is the orbital separation of the two stars from pair A, v_∞ is the W-R wind terminal velocity, \dot{M} is the W-R mass-loss rate, i is the orbital inclination of pair A, and ϕ is the orbital phase. All data sets were initially brought to the same reference point, so that m_0 vanishes in equation (1). This zero point was calculated for each data set by averaging all data between phases 0.3 and 0.7 in the pair A ephemeris. All data were fitted simultaneously for the inclination, the mass-loss rate, and a possible period variation \dot{P} . After a preliminary analysis with constant P , the parameter \dot{P} was introduced to account for the dominating effects of mass loss from the W-R star in

TABLE 1
JOURNAL OF SPECTROSCOPIC OBSERVATIONS OF GP CEP

HJD (2,451,000.0+) (1)	PHASE		W-R χ -CORRELATION ^a (4)	OB RADIAL VELOCITY (km s ⁻¹)			
	Pair A 6.6884 (days) (2)	Pair B 3.4696 (days) (3)		χ -Correlation ^b (5)	λ 4541 ^c (6)	λ 4471 ^d (7)	λ 4920 ^e (8)
348.7441.....	0.034	0.627	295	-88	-162	-155	-163
349.7623.....	0.186	0.921	456	-120	n/a	-162	-154
350.6592.....	0.320	0.179	444	-50	-167	-59	-32
350.6961.....	0.326	0.190	425	-58	-154	-37	-29
350.7345.....	0.331	0.201	418	-55	-164	-45	-21
350.7714.....	0.337	0.212	428	-25	-123	-6	-11
351.6748.....	0.472	0.472	228	-17	-85	-101	-82
351.7126.....	0.478	0.483	214	-22	-99	-92	-100
351.7395.....	0.482	0.491	211	-14	-82	-104	-98
352.6273.....	0.614	0.747	-6	-47	-61	-175	-204
352.6550.....	0.619	0.755	0	-34	-33	-127	-200
352.6814.....	0.622	0.762	-8	-34	-55	-160	-208
352.7653.....	0.635	0.786	-15	-23	-15	-136	-170
352.7933.....	0.639	0.794	-32	-30	-40	-141	-197
353.6194.....	0.763	0.033	-36	-5	-58	-67	-86
353.6474.....	0.767	0.041	-30	1	-40	-58	-101
354.7654.....	0.934	0.363	144	21	-32	-51	-48
356.6295.....	0.213	0.900	469	-130	-165	-200	-190
356.6541.....	0.216	0.907	484	-111	n/a	-172	-179
356.6939.....	0.222	0.919	481	-109	-155	-179	-191
356.7701.....	0.234	0.941	493	-95	n/a	-161	-202
356.7967.....	0.238	0.948	495	-87	-130	-149	-159
380.6119.....	0.798	0.812	28	-18	-26	-186	-200
380.6381.....	0.802	0.820	24	-23	-52	-203	-199
380.6656.....	0.806	0.828	33	-19	-30	-204	-198
380.7059.....	0.812	0.839	28	-31	-50	-179	-209
380.7316.....	0.816	0.847	23	-35	-68	-173	-214
380.7581.....	0.820	0.854	24	-32	n/a	-164	-205
380.8230.....	0.830	0.873	1	-61	-79	-188	-227
381.6057.....	0.947	0.099	192	36	-9	-42	-64
381.6322.....	0.951	0.106	206	45	4	-44	-61
381.6840.....	0.959	0.121	199	32	-10	-10	-54
381.7381.....	0.967	0.137	238	61	37	-7	0
381.7641.....	0.971	0.144	234	59	27	-21	-7
381.8257.....	0.980	0.162	224	35	-37	-14	-22
382.7273.....	0.115	0.422	419	-34	n/a	-114	-78
382.7610.....	0.120	0.432	427	-34	-152	-99	-95
382.8123.....	0.127	0.447	445	-32	-137	-69	-110
383.5825.....	0.243	0.668	487	-135	n/a	-219	-194
383.6093.....	0.247	0.676	475	-144	-198	-209	-217
383.6411.....	0.251	0.685	468	-142	-197	-215	-225
383.6950.....	0.259	0.701	458	-144	-158	-238	-228
386.6611.....	0.703	0.556	-9	35	50	-109	-103
386.6909.....	0.707	0.564	3	37	n/a	-88	-119
386.7201.....	0.712	0.573	2	31	13	-74	-135
387.6745.....	0.854	0.848	71	3	-37	-172	-182
387.7102.....	0.860	0.858	73	-4	-35	-156	-153
387.7494.....	0.866	0.869	82	-8	-50	-132	-144
387.8130.....	0.875	0.888	96	-3	-97	-103	-168
389.5727.....	0.138	0.395	492	-17	-158	-43	-54
389.6036.....	0.143	0.404	493	-22	-184	-49	-69
389.6474.....	0.149	0.416	500	-30	-161	-59	-91
390.5752.....	0.288	0.684	445	-144	-175	-243	-238
390.6109.....	0.293	0.694	441	-139	-160	-206	-227
390.6608.....	0.301	0.709	445	-136	-184	-209	-223
390.7367.....	0.312	0.730	451	-128	-181	-199	-211
390.7889.....	0.320	0.746	449	-132	-165	-199	-227
390.8152.....	0.324	0.753	421	-147	-189	-208	-240
440.5496.....	0.760	0.087	-4	53	-55	-19	-22
440.5768.....	0.764	0.095	-2	56	-30	-14	-35

TABLE 1—Continued

HJD (2,451,000.0+) (1)	PHASE		W-R x-CORRELATION ^a (4)	OB RADIAL VELOCITY (km s ⁻¹)			
	Pair A 6.6884 (days) (2)	Pair B 3.4696 (days) (3)		x-Correlation ^b (5)	λ 4541 ^c (6)	λ 4471 ^d (7)	λ 4920 ^e (8)
440.6037.....	0.768	0.103	7	64	-25	-15	-21
440.6303.....	0.772	0.111	17	71	-10	10	-10
440.6565.....	0.776	0.118	27	76	-9	17	-6
440.6827.....	0.780	0.126	37	82	-44	31	1
440.7085.....	0.784	0.133	52	89	-24	22	19
440.7345.....	0.788	0.141	58	103	16	28	26
440.7612.....	0.792	0.148	33	73	-1	15	0
440.7883.....	0.796	0.156	37	78	-15	12	3
440.8148.....	0.800	0.164	38	77	-79	32	1
440.8440.....	0.804	0.172	27	51	-65	4	-6
441.5351.....	0.907	0.371	145	32	n/a	-29	-15
449.5225.....	0.101	0.673	415	-56	-120	-145	-137
449.5868.....	0.111	0.692	453	-48	-118	-136	-155
449.6516.....	0.121	0.711	463	-55	-110	-145	-169
449.7068.....	0.129	0.727	454	-77	-99	-157	-186
449.7591.....	0.137	0.742	478	-68	-107	-134	-165
449.8355.....	0.148	0.764	479	-93	-160	-164	-185
450.5411.....	0.254	0.967	523	-31	n/a	-114	-97
450.5708.....	0.258	0.976	516	-34	n/a	-101	-114
450.6061.....	0.263	0.986	517	-29	n/a	-89	-99
450.6382.....	0.268	0.995	521	-16	n/a	-95	-75
450.6684.....	0.273	0.004	531	-0	n/a	-60	-56
450.6987.....	0.277	0.013	524	-27	n/a	-91	-88
452.8114.....	0.593	0.622	46	-25	n/a	-98	-117
452.8496.....	0.599	0.632	40	-27	n/a	-88	-128
453.5000.....	0.696	0.820	-18	-16	-46	-132	-110
453.5437.....	0.703	0.833	-21	-13	-50	-146	-135
453.5889.....	0.709	0.846	-18	-11	-36	-121	-139
453.6439.....	0.718	0.861	10	10	-20	-132	-91
453.6732.....	0.722	0.870	0	-0	-50	-107	-104
453.7097.....	0.727	0.880	8	5	-8	-90	-148
453.7369.....	0.732	0.888	4	-2	-29	-131	-131
471.4577.....	0.381	0.996	432	-4	-76	-63	-61
471.5106.....	0.389	0.011	396	-12	-90	-65	-71
473.4446.....	0.678	0.568	2	22	10	-65	-96
473.5273.....	0.690	0.592	7	26	17	-102	-113
473.5725.....	0.697	0.605	24	50	82	-72	-81
473.6088.....	0.703	0.616	5	34	31	-111	-104
473.7349.....	0.722	0.652	19	29	35	-93	-122

^a $\sigma = 4 \text{ km s}^{-1}$.

^b $\sigma = 19 \text{ km s}^{-1}$.

^c Some spectra not well restored for this line were not used; $\sigma = 10 \text{ km s}^{-1}$.

^d $\sigma = 11 \text{ km s}^{-1}$.

^e $\sigma = 9 \text{ km s}^{-1}$.

pair A. The W-R terminal velocity was taken from Prinja, Barlow, & Howarth (1990), $v_{\infty} = 1785 \text{ km s}^{-1}$. The intensity ratio was calculated from the values found in § 3.4:

$$\frac{I_{\text{W-R}} + I_{\text{B}_1} + I_{\text{B}_2}}{I_{\text{A}}} = 1.3. \quad (4)$$

The value $a \sin i = 35.2 R_{\odot}$ was estimated by fitting the radial velocity curve of the W-R component (see § 3.3). The phase was computed from the decimal part of the formula

$$\phi_{\text{A}} = \frac{\text{HJD} - T_{0,\text{A}}}{P_{0,\text{A}} + \dot{P}(\text{HJD} - T_{0,\text{A}})}, \quad (5)$$

where $T_{0,\text{A}}$ and $P_{0,\text{A}}$ are the ephemeris of Massey (1981).

The light curve of pair B was fitted using the superposition of two models represented by equation (1), one being translated by 0.5 in phase. Pair B is a photospheric eclipsing system, so there is no *physical* justification for the use of this equation. Nevertheless, its general *mathematical* form provides a useful means to fit the light curve in pair B:

$$m = m_0 + A_1 \left(\frac{\pi/2 + \arcsin \epsilon_1}{\sqrt{1 - \epsilon_1^2}} \right) + A_2 \left(\frac{\pi/2 + \arcsin \epsilon_2}{\sqrt{1 - \epsilon_2^2}} \right), \quad (6)$$

with

$$\epsilon_1 = B \cos 2\pi\phi_B, \quad \epsilon_2 = B \cos 2\pi(\phi_B - 0.5). \quad (7)$$

The formal fitted parameters are then A_1 , A_2 , B , and m_0 . Contrary to pair A, m_0 is allowed here to vary from epoch to epoch, to compensate for any influence of pair B's eclipses when fitting the light curve of pair A in the early stage of convergence.

All fits were done using a genetic algorithm. This type of algorithm is easy to implement, enabling one to efficiently search a large portion of parameter space. The GALib genetic algorithm package, written by Matthew Wall at the Massachusetts Institute of Technology, was used.³ The pro-

cedure χ^2 converged after three iterations, providing two separated light curves. The result of the last iteration is presented in Figure 2, with the estimated parameters in Table 2.

The approach taken here, namely a two-stage iterative technique, has the advantage of having fewer parameters than a global simultaneous fit to the light curve and thus converges quickly. A simultaneous general least-squares fit could have been carried out but in light of the satisfactory results was deemed unnecessary.

For pair A, we find an inclination of $72^\circ.7 \pm 0^\circ.4$ and a mass-loss rate of $(0.75 \pm 0.02) \times 10^{-5} M_\odot \text{ yr}^{-1}$. The first value is comparable, although not strictly compatible, to those found from their photometry by Lamontagne et al. (1996), $74^\circ.0 \pm 0^\circ.7$, and from broadband polarimetry by St-Louis et al. (1988), $78^\circ.2 \pm 1^\circ.0$. Note that Polyakova (1993) deduced from its photometry and polarimetry a value

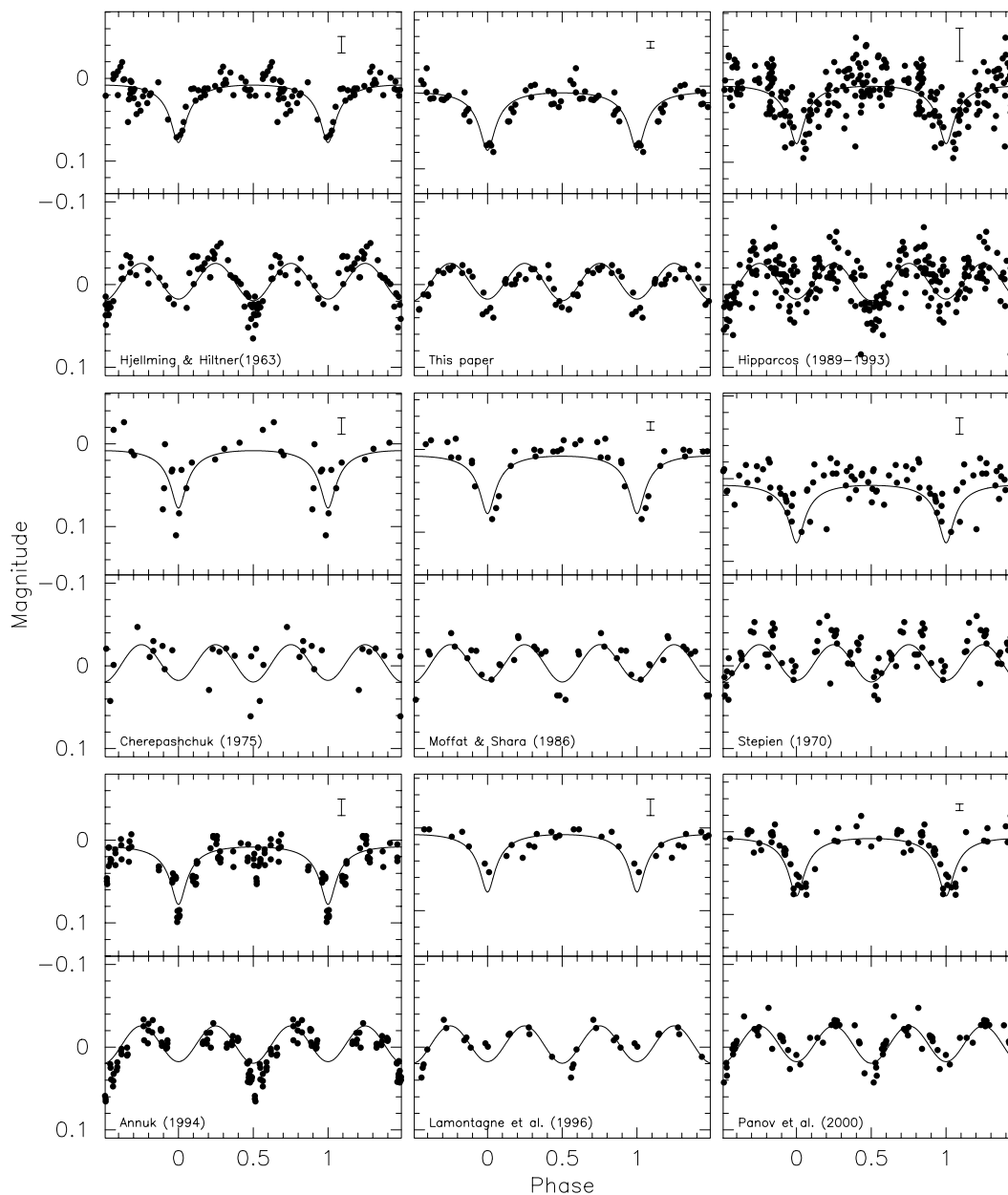


FIG. 2.—Light-curve fit of all available photometric data sets after three iterations (see text). Each section presents pair A and pair B light curves, respectively. All data sets were fitted simultaneously. Here 2σ error bars are given in the top right corner of each panel. These error bars are observational errors as stated by the various authors.

³ See <http://lancet.mit.edu/ga>.

$i = 65^\circ$. This places our estimate roughly in the middle of the observed range. The fit also shows that there is a period variation of $+1.3 \pm 0.2 \text{ s yr}^{-1}$ for pair A. This transforms the period found by Massey in 1979 to 6.6887 ± 0.0001 days for 1999, the time of our spectroscopic data. Choosing cycle number $E = 1145$ from 1999 as an arbitrary but convenient reference, the corresponding extrapolated time of conjunction is $T_{0\text{pres}} = 2,443,690.32 + PE + 0.5PPE^2 = 2,451,348.72$. The period variation is presumably caused by mass loss mainly from the W-R star. Khaliullin (1974) has shown that the mass-loss rate can be derived from \dot{P} within a factor of 3 if $Q \equiv \dot{M}_{\text{W-R}}/M_{\text{O}}$ lies in the range 0.17–0.55, as is the case for GP Cep (see § 3.3). In the most likely case of an isotropic mass outflow from the W-R star and under the assumption of negligible wind from the O companion, one finds

$$\dot{M}_{\text{W-R}} = -\frac{1}{2}(M_{\text{W-R}} + M_{\text{O}})\frac{\dot{P}}{P}. \quad (8)$$

We obtain $\dot{M}_{\text{W-R}} = (2.9 \pm 0.5) \times 10^{-5} M_{\odot} \text{ yr}^{-1}$, which is effectively within a factor of 4 from the above photometric value (see Table 2). We do not have any reason to choose one value of \dot{M} over the other. Both ways of deriving it lead to systematic errors. The light-curve fitting procedure introduces systematic errors caused by strong correlation of the fitted parameters, namely, i and \dot{M} . In the second approach, \dot{M} depends on \dot{P} , which is derived in a more straightforward manner (timing of the light-curve minima). However, the used physical model produces results accurate within a factor of 3. For these reasons, we adopt a range for the mass-loss rate of $(0.8\text{--}3.0) \times 10^{-5} M_{\odot} \text{ yr}^{-1}$. The independent estimate made by St-Louis et al. (1988) from polarimetric observations, $\dot{M}_{\text{W-R}} = 2.5 \times 10^{-5} M_{\odot} \text{ yr}^{-1}$, compares well with our result.

3.2. Spectral Component Separation

The iterative process devised by Marchenko et al. (1998a) to separate components in a W-R+O system uses cross-correlation over the most prominent features of either the W-R component or the OB component to measure an RV shift relative to a template spectrum of either star.

The first step is to obtain the RVs computed by cross-correlating all spectra with one template. This was done using the *fxcor* task of IRAF. The template was chosen to be simply a typical good S/N spectrum. The cross-correlation is first carried out on the most prominent features of the W-R star, i.e., in the range 4545–4820 Å. All the spectra are then shifted to the template’s frame of reference, and a mean spectrum is calculated. This mean W-R spectrum is then brought to the same frame of reference as each original unshifted spectrum using the previously determined shift and subtracted from it. At this stage we have a spectrum of all three OB stars combined, the first-iteration

W-R spectrum having been subtracted out. These steps (cross-correlation, shift, and subtraction) are repeated on all the individual W-R-free spectra but this time using the ranges 4260–4610, 4800–5070, and 5300–5520 Å for cross-correlation, i.e., regions dominated by absorption features. The mean OB star spectrum is calculated and subtracted out from the original W-R+O spectra, giving an improved spectrum of the W-R star. The process is repeated again as many times as necessary to converge to separated W-R and OB spectra.

After 10 iterations, the emission-line profiles no longer change. Figures 1b and 1c show the mean separated spectra for the W-R component and the three combined OB stars, respectively. The error introduced by such a process comes from all the individual errors accumulated while performing the cross-correlation. The major, most apparent effect resulted in a shift of the reconstructed W-R spectrum toward the red. Note, however, that this is only a zero-point shift, which does not change the relative RV measurements.

Attempts were made at separating the three combined OB components. However, none proved successful. The cross-correlation procedure similar to the one applied for the W-R component does not converge in the case of the three blended OB spectra, because it is not possible to construct a template spectrum sufficiently representative of one OB component, whichever it may be. Our spectra do not cover enough epochs to be able to separate three components, one of which, the OB companion of pair A, is not distinguished from the other two. However, some conclusions can still be made about the orbital parameters and spectral types.

Another effect may influence the separation procedure, making it more complex, namely, the period P_b being close to $P_a/2$. This inevitably causes some phase grouping that, although not so severe (see the subpanels in Fig. 3 for the phase distributions of the residuals), nevertheless may have some influence on the attempt to disentangle the OB components.

3.3. Orbital Elements

3.3.1. W-R Component

The process by which the spectra of the OB components were subtracted out directly provides the RVs of the W-R star. Orbital elements were derived by applying the least-squares fit algorithm of Bertiau, Grobben, & Grobben (1969). They are $P = 6.6906 \pm 0.0021$ days, $K = 255 \pm 2 \text{ km s}^{-1}$, $T_{0,A} = \text{HJD } 2,451,348.89 \pm 0.02$, $a \sin i = 35.2 R_{\odot}$, and $e = 0.05 \pm 0.01$. The systemic velocity (γ) of the W-R component was arbitrarily brought to zero, as this orbital parameter cannot be restricted by RV measurements of the lines formed in the rapidly expanding W-R wind. The period found here, 6.6906 days, is slightly longer than that derived from the photometric data, 6.6887 days. We prefer the latter because it is derived from the data covering ~ 40 yr and is less prone to systematic errors. A new fit was done, this time fixing $P = 6.6887$ days and $e = 0$. Indeed, seemingly significant but small $e = 0.05$ found for the W-R star can be introduced in the cross-correlation procedure by the unaccounted profile distortions caused by the deep atmospheric eclipse and the wind-wind interaction phenomenon. The new orbital elements are given in Table 3 with formal errors given by the algorithm. No change in the K value was introduced by fixing P and e . The fit is shown in Figure 3

TABLE 2
ESTIMATED PARAMETERS FROM THE LIGHT CURVE OF PAIR A

Inclination (deg)	\dot{M} ($\times 10^{-5} M_{\odot} \text{ yr}^{-1}$)	\dot{P} (s yr^{-1})
72.7 ± 0.4	0.75 ± 0.02	1.3 ± 0.2

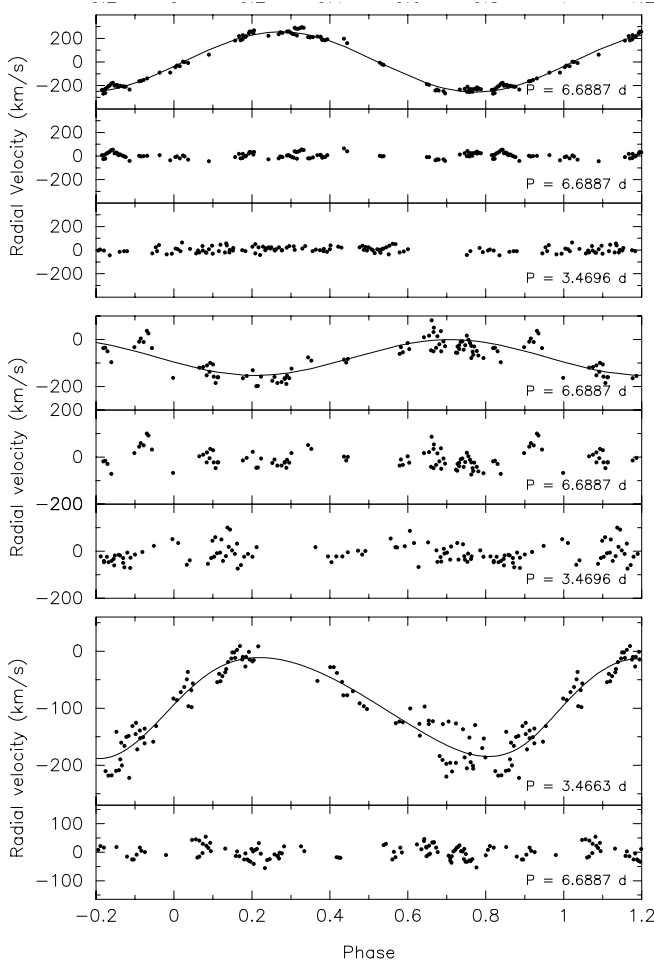


FIG. 3.—*Top*: Radial velocity curve of the W-R component computed from cross-correlation of the $\lambda\lambda 4545\text{--}4820$ region. The typical σ error is 4 km s^{-1} . Residuals are plotted at the bottom as a function of phase for the two periods. *Middle*: Radial velocity curve of the absorption line He II $\lambda 4541$ ($\sigma = 10 \text{ km s}^{-1}$). First tier shows the fit with a fixed period of 6.6887 days and $e = 0.0$; second and third tiers are the residuals phased with both periods 6.6887 and 3.4696 days, respectively. *Bottom*: Radial velocity curve of the He I lines $\lambda\lambda 4471$ and 4921 after correction for the 6.6887 day period residuals along with the fit (*top half*). The bottom half shows the residuals from the top fit, phased with the ephemeris of pair A. The typical σ error is 10 km s^{-1} . Note that the period for pair B here is the fitted value, although we prefer the period from Annuk (1994; see text).

(*top*). It can be seen from the residuals of the velocity curve that there is only one W-R star in this quadruple system, as noted by Massey (1981), but contrary to a previous claim by Panov & Seggewiss (1990). Panov & Seggewiss based their conclusion of two W-R stars solely on the photographic spectroscopic radial velocities for emission lines of Hiltner

(1945). While Hiltner found $K = 245 \text{ km s}^{-1}$ in system A for three emission lines, Panov & Seggewiss found $K = 25 \text{ km s}^{-1}$ in system B after plotting Hiltner's residuals. Since this latter K value is close to the scatter of the RVs, the case for a second W-R star remains unconvincing.

3.3.2. OB Components

Even though the OB components were not separated, it was possible to obtain fairly reliable RVs for one of the pair B stars and for the OB companion of the W-R star by fitting the He I lines $\lambda\lambda 4471$ and 4921 and the He II $\lambda 4541$ line, respectively. The choice of these lines is explained below.

The top panel of Figure 4 shows these lines along with the H β line phased with the 6.6887 day period of pair A. These spectra show the W-R-free OB absorption components obtained from the cross-correlation procedure mentioned above. The bottom panel of Figure 4 shows the same spectra but phased with the 3.4696 day period of pair B. The gray-scale plots of both He I lines depict clear sinusoidal-like curves when phased with the pair B ephemeris, which leads us to conclude that these lines dominate in pair B. Using the centroid method of the IRAF task *splot*, the velocities of the He I lines were computed. The average is shown in Figure 3 (*bottom*), where the 6.6887 days residual fit was subtracted. The orbital elements are given in Table 4, along with their formal errors.

Annuk (1994) obtained $T_{0,B} = \text{HJD } 2,443,689.16$ and $P_B = 3.4696$ days. The expected time of conjunction, $T_{0,\text{pres}} = 2,443,689.16 + 3.4696 \times 2217 = 2,451,381.26$, compares favorably with our estimate, $2,451,381.22 \pm 0.09$. Some bias due to the W-R component separation procedure might explain the difference in period (3.4663 ± 0.0011 in our case). We prefer the period of Annuk that was derived from photometry and not from the fit of only two lines.

It is clear from Figure 4 that the He II absorption line $\lambda 4541$ dominates in pair A. This gray-scale plot shows a \sim sinusoidal curve that is in strong contrast to the erratic behavior of He II $\lambda 4541$ while phased with the ephemeris of pair B. Again, the RV curve was computed and fitted to the He II $\lambda 4541$ line data. This time we held fixed $P = 6.6887$ days and $e = 0$. The resulting fit (see Fig. 3, *middle*, and Table 3) gives a lower limit of the orbital amplitude, from which it is possible to estimate a lower limit for the masses of the stars in pair A: $M_{W-R} \sin^3 i \gtrsim 5.7 M_\odot$, and $M_{O_A} \sin^3 i \gtrsim 19.0 M_\odot$. The mean inclination found from photometry (cf. § 3.1) and from polarimetry by St-Louis et al. (1988) is 75° , which gives $M_{W-R} \gtrsim 6.3 M_\odot$ and $M_{O_A} \gtrsim 21.1 M_\odot$. The mass ratio is $Q \equiv M_{W-R}/M_O = K_O/K_{W-R} \gtrsim 0.3$.

This limit for the mass ratio is lower than that of the two other known Galactic WN6 binaries, which have $Q = 0.85$ and 0.54 (van der Hucht 2001). It is, however, within the range of other WN binaries that have $Q \sim 0.3\text{--}0.6$ (Moffat 1995). Massey (1984) assumed $M_{W-R} = 10\text{--}25 M_\odot$, arguing that for the W-R star to have a mass lower than $10 M_\odot$, the allowed range of inclinations would require a mass ratio lower than 0.4, and that could only be the case if the composite absorption lines were dominated by the O member of pair A, contrary to what he found. Here, the parameters for the OB star of pair A are derived from only one spectral line (He II $\lambda 4541$) shown to dominate in pair A, thus giving a better estimate of the orbital amplitude, although strictly speaking only a lower limit due to possible blending.

TABLE 3
ORBITAL ELEMENTS OF GP CEP, PAIR A
($P = 6.6887$ days, $e = 0.0$)

Element	W-R	O
K (km s^{-1})	$\gtrsim 255 \pm 2$	$\gtrsim 76 \pm 4$
T_0 (2,451,000+)	348.94 ± 0.01	348.76 ± 0.08
$a \sin i$ (R_\odot)	$\gtrsim 35.2$	$\gtrsim 10.5$
γ	Assumed: 0.0	-77 ± 4

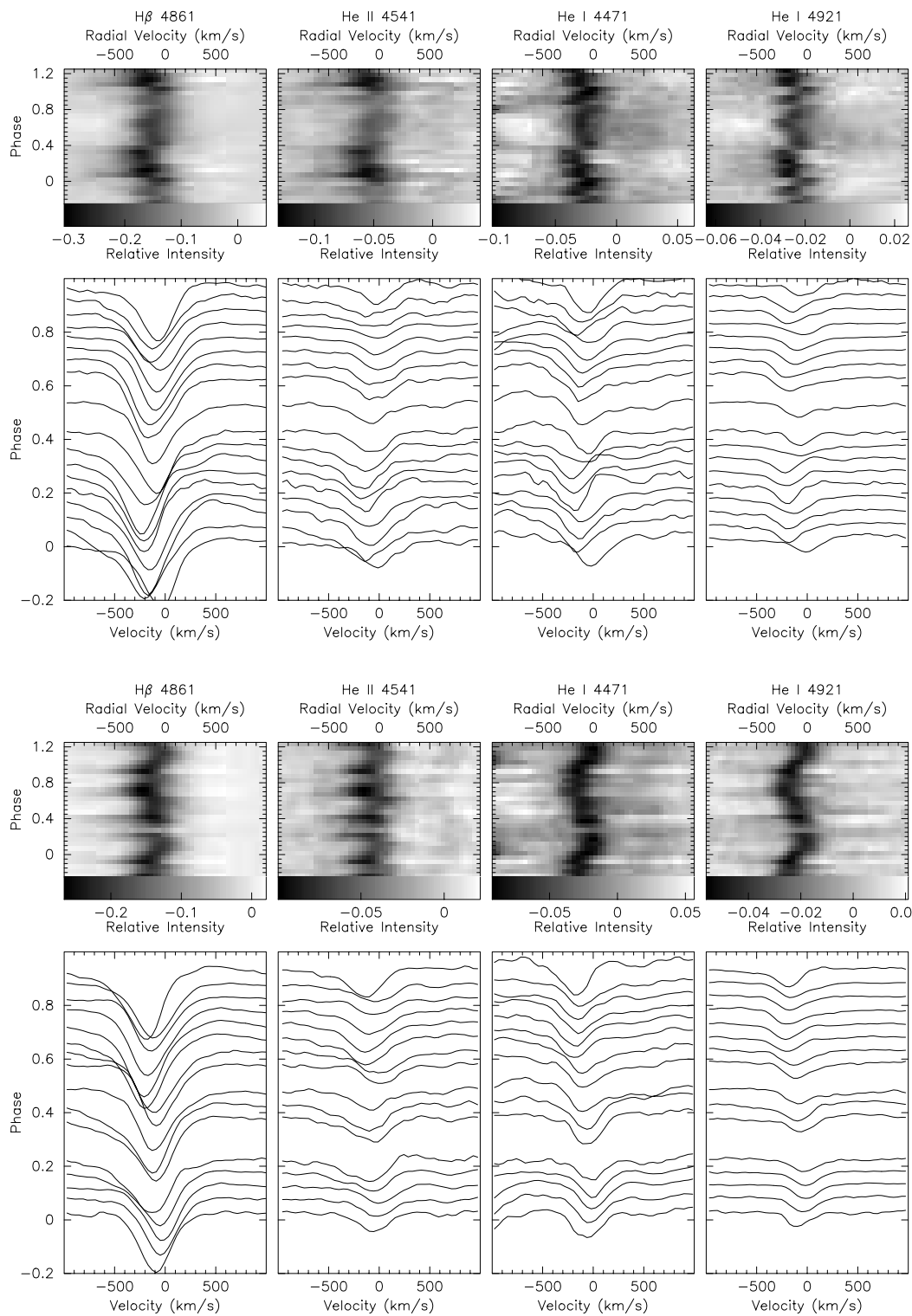


FIG. 4.—Selected absorption lines phased with the 6.6887 day period (*top*) and with the 3.4696 day period (*bottom*). All spectra were averaged in bins of 0.05 in phase.

3.4. Spectral Types

Inspection of the phase-locked RV variations shown in Figure 4 enables us to conclude the following:

1. The He I lines $\lambda\lambda 4471$ and 4921 arise mainly in one star of pair B, hereafter called OB_{B1} .

2. H β is \sim equally present in the O star of pair A, hereafter called O_A , and in either both or one component of pair B.

3. He II $\lambda 4541$ arises mainly in O_A .

It follows from the first statement that there are essentially no detectable lines of neutral helium in the second star of

TABLE 4
ORBITAL ELEMENTS OF THE BRIGHTEST STAR IN PAIR
B (OB_{B1})

Element	Fitted Value
P (days).....	3.4663 ± 0.0011
γ (km s ⁻¹).....	-93 ± 2
K (km s ⁻¹).....	$\geq 87 \pm 2$
T_0	$2,451,381.22 \pm 0.09$
$a \sin i$ (R_\odot).....	≥ 5.9
e	0.16 ± 0.03
$f(m)$ (M_\odot).....	≥ 0.23

pair B, OB_{B2}, or in O_A, i.e., presumably OB_{B1} dominates by luminosity in pair B. From the last statement, it follows that He II is practically absent in both stars of pair B. Table 5 summarizes the situation.

Morgan, Code, & Whitford (1955) classify GP Cep as B0: I+W-R. Indeed, the spectral type B0: I appears to apply very well to OB_{B1}. This type is consistent with the presence of neutral helium and hydrogen and the absence of He II. The luminosity class is consistent with the fact that there is only one star detected in He I. The supergiant's companion is detectable in the light curve of pair B via the secondary eclipse. Because both eclipses are of the same depth, the effective temperatures of both stars in pair B are comparable. It is then possible to assign a rough spectral type to OB_{B2}. The spectral type of a main-sequence or giant star having the same temperature as a supergiant of type B0: I is B1: V–III (Schmidt-Kaler 1982). Thus, for pair B, the proposed spectral types are B0: I + B1: V–III. The approximate absolute visual magnitudes for these spectral types are $M_v = -6$ and -4 , respectively.

As the OB_{B1} component dominates by luminosity in pair B, then the H β line traces the motion of two stars, O_A and OB_{B1}. Since the equivalent width of the H β line supposedly correlates with M_v (Millward & Walker 1985), the visual magnitude of O_A can be crudely estimated as $M_v \simeq -6$, i.e., comparable to the M_v of the OB_{B1} component. Furthermore, OB stars that show He II lines that are stronger than He I lines and that have absolute visual magnitudes in the observed range are of type O3–6 (Walborn & Fitzpatrick 1990). The adopted spectral type of the W-R star is WN6o/WCE (Smith et al. 1996). The absolute magnitude given by van der Hucht (2001) for a WN6 star is $M_v = -4$. For pair A, the spectral type is then WN6o/WCE + O3–6. Table 5 gives all proposed spectral types along with their absolute visual magnitudes.

TABLE 5
QUALITATIVE LINE STRENGTHS AND PROPOSED APPROXIMATE SPECTRAL
TYPES WITH ABSOLUTE MAGNITUDES

STAR	LINES			SPECTRAL TYPE	M_v
	H I	He I	He II		
O _A	Present	Weak	Dominant	O3-6	-6
OB _{B1}	Present	Dominant	Weak	B0: I	-6
OB _{B2}	Present?	Weak	Weak	B1: V–III	-4
W-R.....	n/a	n/a	n/a	WN6o/WCE	-4

3.5. Wind-Wind Collision in Pair A of GP Cep

One of the signatures of a wind-wind collision is phase-dependent excess emission, as seen in the well-known WN5+O6 eclipsing binary V444 Cyg (Marchenko et al. 1997). Their Figure 6 gives the residuals, individual spectra minus mean, of the He I $\lambda 4471$ and He II $\lambda 4686$ lines in V444 Cygni. In V444, the excess emission originates in the arms of the bow shock zone relatively far from the head. It is best seen in the He II $\lambda 4686$ line as a traveling emission peak that splits into two partially overlapped subpeaks around phase 0.125–0.325 and 0.775–0.875, representing the leading and trailing bow shock arms. These arms are also detected in absorption in He I, which appears for the first time around phase 0.3 and grows stronger toward $\phi = 0.5$, then is depleted around $\phi = 0.6$ and increases sharply at $\phi = 0.73$. The geometry of the system helps to interpret these additional absorption components as arising as a result of the projections of initially the leading, and afterward the trailing, bow shock arm on the bright disk of the O companion. Another interesting feature is a blueshifted absorption in He I $\lambda 4471$ at phase 0.9. It has no counterpart at phase 0.1, as might be expected if due to an atmospheric eclipse, i.e., as due to the absorption of the O star companion light by the W-R wind at the orbital phases when the O star passes behind the W-R component. No plausible explanation of the origin of this phase-shifted absorption feature has been given to date. Finally, there is a long-lasting atmospheric eclipse in He II $\lambda 4686$ for V444 Cyg. It starts at phase $\phi \sim 0.75$ and ends at $\phi \sim 0.25$.

Figure 5 shows the residual (individual spectra minus mean spectrum) features emerging from the colliding winds in pair A of GP Cep. All spectra were brought into the same frame of reference and corrected for the continuum variation using the formula $10^{-0.4[m_v(\phi) - m_v(\max)]}$ (Morel, St-Louis, & Marchenko 1997), where $m_v(\phi)$ and $m_v(\max)$ are the magnitude at a given phase and at the maximum of the light curve of pair A, respectively. A mean spectrum consisting of all spectra except those at $0.8 < \phi < 1.2$ and $0.7 < \phi < 0.75$ was constructed. The spectra in this first range of phases were rejected because of the atmospheric eclipse and in the second range because of the presence of an abnormally strong absorption in He I. The spectra in Figure 5 were averaged in bins of 0.05 in phase. The only excess emission is seen in He II $\lambda 4686$ as a small, blueshifted (~ -400 km s⁻¹) phase-locked peak first appearing at phase $\phi \sim 0.4$. It stays there until $\phi \sim 0.6$, disappears, and shows up again at $\phi \sim 0.7$, but now redshifted to $+400$ km s⁻¹. However, this emission appears to be relatively stable and short lived, in contrast to a *continuously shifting emission peak* as in V444 Cyg. The seeming stability can be caused by the bias introduced during the subtraction of the average W-R spectrum, as the extra emission component, being transmitted to the average spectrum, tends to produce, although being relatively weak, some small but noticeable depressions at the corresponding wavelengths in Figure 5, cf. $\phi = 0.325$, 0.625–0.675. Such overestimation of the intensity in the average W-R profile may even offset the probable rise of the extra emission at phases as early as $\phi \sim 0.25$.

More interesting is the behavior of the absorption features in He I $\lambda 4471$. The absorptions seen in V444 Cyg at $\phi \simeq 0.725$ and $\phi \simeq 0.925$ are also seen in GP Cep at exactly the same phases. There is some hint of an absorption originating in the leading arm but seen earlier ($\phi \sim 0.275$) than

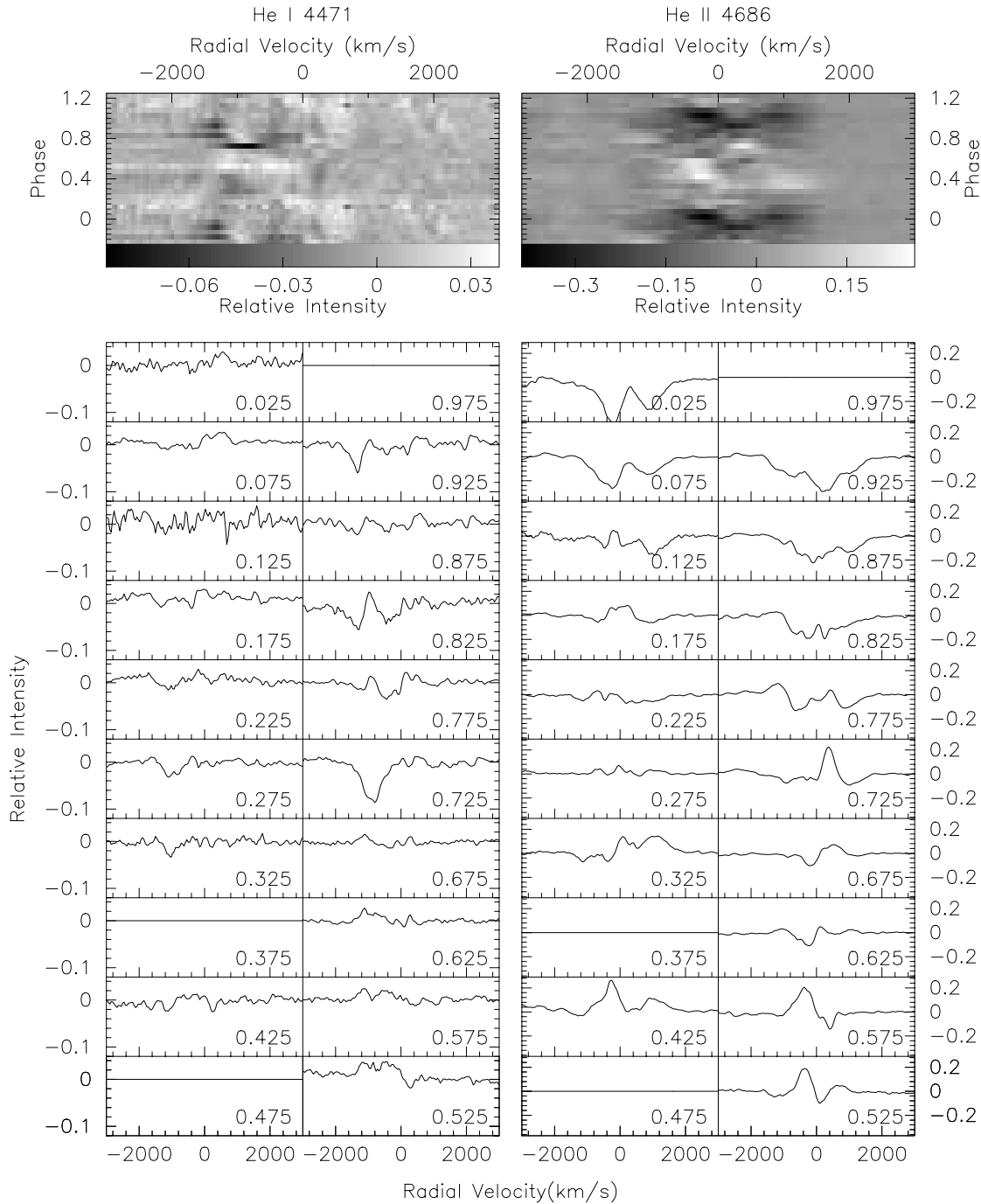


FIG. 5.—Residual features emerging from the colliding winds in pair A of GP Cep. Shown are gray-scale plots of He I $\lambda 4471$ and He II $\lambda 4686$ (top) and conventional style plot of the same lines (bottom). The midphases of the 0.05 phase bins are indicated in the bottom right corner.

in V444 Cyg ($\phi \sim 0.35$). This could be due to a wider cone-opening angle [$\dot{M}_{W-R}v_{\infty}(W-R)/\dot{M}_{O}v_{\infty}(O)$ is presumably lower than in V444 Cyg] combined with a smaller coriolis shift of the shock cone and/or a wind-braking mechanism more efficient in GP Cep than in V444 Cyg (see § 3.6).

Tracing the phase-dependent behavior of the He II line, we conclude that there are some WWC effects in GP Cep, but on a much weaker scale than in V444 Cygni. While the appearance of the strong He I absorption component at $\phi = 0.72$ can be taken as solid evidence in favor of the presence of a bow shock, the weak additional emission in He II can be interpreted as not only arising in the bow shock arms,

but also due to the presence of the luminous, hot, close companion as an external source of illumination. This might be especially true when considering the asymmetric shape of the atmospheric eclipse in He II. GP Cep's W-R star is of subtype WN6, cooler than the WN5 component in V444 Cyg, and GP Cep's O_A star may be hotter. Conceivably, this excess emission could be caused by the hot luminous O star irradiating the W-R wind. The atmospheric eclipse is asymmetric, with the maximum absorption displaced toward the red. This implies that the He II zone is extended toward the O star, the source of additional excitation in the close A pair (see Fig. 6).

wind-wind collision zone (see Fig. 6 and the blue-red asymmetry of the atmospheric eclipse at $\phi \sim 0$), which is suggestive of the same enhancement in He III. Even if He II is the dominant species, detailed ionization equilibria that are not sensitive to density will also yield a ρ^2 emissivity in the $\lambda 4686$ line. Hence, to make further progress, we assume this emissivity scaling.

The emissivity determines the emergent intensity profile in a way that depends in general on the direction cosine μ . The angular dependence is qualitatively different depending on whether the line is thick or thin, so we consider these limits separately.

3.6.2. Radiative Braking Diagnostics for Optically Thin Lines with ρ^2 Emissivity

If the line is thin, the emission escapes isotropically, so the radiative intensity integrated between ν and $\nu + d\nu$ obeys

$$I(\nu, \mu) d\nu \propto \rho^2 dr. \quad (12)$$

The spatial interval dr maps into the observed frequency interval $d\nu$ in a manner regulated by

$$\frac{d\nu}{dr} = \mu \frac{\nu_0}{c} \frac{d\nu}{dr} \propto \frac{\mu}{v}, \quad (13)$$

where ν_0 is the line-center frequency of the transition, and we have used $dv/dr \propto 1/v$ from above. Since $\rho \propto 1/v$ as well, we then have

$$I(\nu, \mu) \propto \frac{1}{\mu v}, \quad (14)$$

and since μv is proportional to the frequency shift from line center $\Delta\nu$, this implies finally that for optically thin “density-squared” lines, the radiative-braking signature would obey

$$I(\nu, \mu) \propto \frac{1}{\Delta\nu}. \quad (15)$$

An important aspect of equation (15) is that it is independent of μ . This does not imply that the profile appears the same from all directions, because the limits on $\Delta\nu$ for which this expression applies will be a function of μ . Specifically, $\Delta\nu$, in velocity units, will vary only between μv_{\min} and μv_{\max} , where v_{\min} and v_{\max} are, respectively, the minimum and maximum speeds of the flow in the braking layer. Note that v_{\max} might normally be equated to the terminal speed of the wind prior to braking, and v_{\min} would be the speed to which the wind brakes before entering a hydrodynamic shock.

It is informative to integrate the intensity over frequency to constrain the equivalent width, yielding a result proportional to

$$\int_{\mu v_{\min}}^{\mu v_{\max}} \frac{d\nu}{\nu} = \log \frac{v_{\max}}{v_{\min}}. \quad (16)$$

This is *also* independent of μ , as it must be for optically thin emission. Thus, although the location of the edges of the profile depends on μ , as seen from the integration limits in equation (16), the frequency-integrated intensity itself does *not* depend on μ for a thin line. High spectral resolution is therefore needed to see the signature of the μ dependence in

this case, to resolve the narrow spiky profiles that should appear near $\mu = 0$ when looking tangential to the braking plane (near phases 0.25 or 0.75) from the broad but weak profiles expected near phase 0.5 (note that the emission at phase 0 is likely to be occulted by the W-R wind).

3.6.3. Optically Thick Recombination Lines

For thick lines, the analysis is quite similar to the above, except for the important difference that substantial photon scattering will occur within the Sobolev region. Assuming that most of these photons do eventually escape in the line, this will primarily only alter the angular dependence of the emergent intensity. In Sobolev theory, this angular dependence is simply proportional to the line-of-sight velocity gradient. Since the line-of-sight gradient is proportional to μ^2 in a plane-parallel model, this implies that the optically thick intensity will mimic the thin case of equation (15), except for the inclusion of the flux-normalized factor $\mu^2/4$, so in unnormalized form,

$$I(\nu, \mu) \propto \frac{\mu^2}{\Delta\nu}. \quad (17)$$

Thus, unlike for the thin case, here the flux preferentially emerges parallel and antiparallel to the flow direction entering the braking layer. The frequency-integrated intensity is then also proportional to μ^2 , so it should show a clear modulation with orbital phase. Since $\Delta\nu \propto \mu v$, equation (17) indicates that the peak intensity scales as μ , whereas the equivalent width scales even more sensitively, as μ^2 . Thus, optically thick emission is both narrow and weak near phases 0.25 and 0.75 but becomes broader and much stronger, and so easier to detect, near phase 0.5.

3.6.4. Discussion for Recombination Lines in GP Cep

These results show that lines with emissivities that scale with ρ^2 formed in a braking layer with fixed ρL should exhibit the signature of a truncated $1/\Delta\nu$ shape, extending between frequencies corresponding to μv_{\min} and μv_{\max} . The wedge shape of such profiles should provide a distinguishable signature when the detection is firm. Optically thin lines may show a very pronounced peak near line center when looking along the face of the braking layer, whereas optically thick lines should be most noticeable when looking directly into the flow, at which point they reach their peak intensity and extend almost to the peak flow speed.

Figure 7 indeed indicates a wedgelike feature in the He II $\lambda 4686$ profile around phase 0.5, which extends to at least 1000 km s^{-1} toward the observer. It is tempting to identify this with the radiative braking signature of an optically thick recombination line. Certainly, this is a speculative association, since the signal is fairly weak and other possible sources have not been ruled out. An important ramification of the presence of radiative braking is that the decelerated wind generates a much lower temperature shocked zone, and this would be expected to substantially reduce the hard X-ray flux normally associated with wind collision. In fact, since the presence of a hard X-ray source could strip the incident wind of the line opacity necessary to induce braking, similar to the Hatchett-McCray effect (Hatchett & McCray 1977), braking may be required to self-perpetuate. To know whether or not this is possible in practice would require a stability analysis that may depend on details such

as where the braking occurs and is beyond the current scope.

Also, the analysis given here is complicated by neglected factors such as eclipsing by the O star, orbital coriolis effects, ionization changes, spherical divergence of wind streams, and curvature of the braking domain. Nevertheless, this simplified first analysis indicates a possible new diagnostic for the presence of radiative braking and associated system constraints. Further quantification by numerical simulation is needed, as is a broader observational survey, to determine the validity and applicability of this diagnostic.

It would be especially telling to find similar diagnostics in other short-period colliding-wind binaries or in other lines from GP Cep. In this regard, it is significant that the He I $\lambda 4471$ line in Figure 7 shows neither a strong nor a wedge-shaped signal, and this presents a challenge to the radiative-braking interpretation. Apparently, considerable He reionization will be required if the wedge-shaped peak in the $\lambda 4686$ residuals near phase 0.5 is to be explained by a braking layer. The most probable source of this reionization in the vicinity of the bow shock head could be the strong radia-

tion field of the hot O_A companion or X-rays from the shock zone itself.

4. SUMMARY

For the quadruple massive binary GP Cep, new photometric data were obtained and combined with all available previous data to derive a new period of 6.6887 days for the W-R star, a new estimate of the W-R mass-loss rate, $(0.8\text{--}3.0) \times 10^{-5} M_{\odot} \text{ yr}^{-1}$, a rate of period variation of 1.3 yr^{-1} , and an orbital inclination of $72^{\circ}7$ for pair A. With all spectroscopic and photometric data combined, new masses are proposed for pair A: $\geq 6 M_{\odot}$ and $\geq 21 M_{\odot}$ for the W-R and O stars, respectively. New spectral types are proposed for all three OB components in this quadruple system: O3–6 for the O star in pair A, and B0: I and B1: V–III for the stars in pair B.

By separating the W-R spectra from the three combined O star spectra, it was possible to study the WWC effects in GP Cep. We show that those effects are much less pronounced than in V444 Cygni, if present at all. Certain signatures of radiative braking may also be present.

REFERENCES

- Annuk, K. 1994, *A&A*, 282, 137
 Bertiau, F., Grobбен, S., & Grobбен, J. 1969, *Ricerche Astron.*, 8, 1
 Cherepashchuk, A. M. 1975, *AZh*, 52, 255
 De Marco, O. 2002, in *ASP Conf. 260, Interacting Winds from Massive Stars*, ed. A. F. J. Moffat & N. St-Louis (San Francisco: ASP), 517
 Gayley, K. G., Owocki, S. P., & Cranmer, S. R. 1997, *ApJ*, 475, 786
 Hatchett, S., & McCray, R. 1977, *ApJ*, 211, 552
 Hiltner, W. A. 1945, *ApJ*, 101, 356
 Hjellming, R. M., & Hiltner, W. A. 1963, *ApJ*, 137, 1080
 Kaufer, A. 2002, in *ASP Conf. 260, Interacting Winds from Massive Stars*, ed. A. F. J. Moffat & N. St-Louis (San Francisco: ASP), 489
 Khaliullin, K. F. 1974, *AZh*, 51, 395
 Lamontagne, R., Moffat, A. F. J., Drissen, L., Robert, C., & Matthews, J. M. 1996, *AJ*, 112, 2227
 Marchenko, S. V., Moffat, A. F. J., & Eenens, P. R. J. 1998a, *PASP*, 110, 1416
 Marchenko, S. V., Moffat, A. F. J., Eenens, P. R. J., Cardona, O., Echevarria, J., & Hervieux, Y. 1997, *ApJ*, 485, 826
 Marchenko, S. V., et al. 1998b, *A&A*, 331, 1022
 Massey, P. 1981, *ApJ*, 244, 157
 ———. 1984, *ApJ*, 281, 789
 Millward, C. G., & Walker, G. A. H. 1985, *ApJS*, 57, 63
 Moffat, A. F. J. 1995, in *IAU Symp. 163, Wolf-Rayet Stars: Binaries; Colliding Winds; Evolution*, ed. K. A. van der Hucht & P. M. Williams (Dordrecht: Kluwer), 213
 Moffat, A. F. J., & Shara, M. M. 1986, *AJ*, 92, 952
 Morel, T., Georgiev, L. N., Grosdidier, Y., St-Louis, N., Eversberg, T., & Hill, G. M. 1999, *A&A*, 349, 457
 Morel, T., St-Louis, N., & Marchenko, S. V. 1997, *ApJ*, 482, 470
 Morgan, W. W., Code, A. D., & Whitford, A. E. 1955, *ApJS*, 2, 41
 Panov, K. P., Altmann, M., & Seggewiss, W. 2000, *A&A*, 355, 607
 Panov, K. P., & Seggewiss, W. 1990, *A&A*, 227, 117
 Perryman, M. A. C. 1997, *The Hipparcos Catalogue (ESA SP-1200; Noordwijk: ESA)*
 Polyakova, T. A. 1993, *Astron. Rep.*, 37, 165
 Prinja, R. K., Barlow, M. J., & Howarth, I. D. 1990, *ApJ*, 361, 607
 Schmidt-Kaler, T. 1982, *Landolt-Börnstein, New Series, Group 6*, ed. K. Schaiffers & H. H. Voigt, Vol. 2b (Berlin: Springer), 1
 Smith, L. F., Shara, M. M., & Moffat, A. F. J. 1996, *MNRAS*, 281, 163
 Stepien, K. 1970, *Acta Astron.*, 20, 117
 St-Louis, N., Moffat, A. F. J., Drissen, L., Bastien, P., & Robert, C. 1988, *ApJ*, 330, 286
 van der Hucht, K. A. 2001, *NewA Rev.*, 45, 135
 Walborn, N. R., & Fitzpatrick, E. L. 1990, *PASP*, 102, 379